# Active magnetic sensing for subterranean urban target discrimination

Wilson Ezequelle<sup>a</sup>, Daniel Orfeo<sup>a</sup>, Dylan Burns<sup>a</sup>, Tian Xia<sup>a</sup>, and Dryver Huston<sup>a</sup>

<sup>a</sup>University of Vermont, 33 Colchester Ave., Burlington VT, USA

## ABSTRACT

Location and identification of subterranean infrastructure is crucial for managing and maintaining urban infrastructure and utility, and locating subsurface hazards. Low-frequency oscillating magnetic fields suffer less attenuation due to propagating media than ground penetrating radar. Here, electronically-geared, rotating neodymium magnets project oscillating magnetic fields which are manipulated to provide object identification from rapid analysis of dynamic magnetometer data. Ferromagnetic materials interact directly with the rotating magnetic field. Eddy currents, which induce a counter-propagating magnetic field, are generated in conductive, non-ferromagnetic materials. Two applications are highlighted by preliminary experiments: discrimination between copper, aluminum and steel pipes, and improved detection of buried explosive devices.

**Keywords:** magnetic sensing, eddy currents, target discrimination

#### 1. INTRODUCTION

Object detection and the ability to gain information about an object through non-contact sensing has implications for both modern infrastructure technologies and for locating concealed explosive devices. Many utility maps have large uncertainties pertaining to exact location of subterranean infrastructure. Providing an accurate location and information about the material of the infrastructure under investigation can rapidly improve mapping and excavation processes. Anti-personnel landmines also provide a large challenge to remote sensing techniques as differentiation from natural objects, such as rocks, can be difficult if the natural feature is similar in geometry. Ground penetrating radar emits and receives high frequency electromagnetic fields in order to detect dielectric changes. In many cases, especially with electrically conductive soils, it can be difficult to use ground penetrating radar to gain information about the subsurface feature being sensed. However, data processing techniques such as utilizing phase information have had some success in distinguishing between materials.<sup>1</sup> Methods for identification of antipersonnel landmines have also had some success through extensive data processing of the ground penetrating radar data.<sup>2</sup> A magnetic sensing system may allow for more information about the target to be gained with limited data processing.

Low-frequency magnetic sensing may be able to provide information about different objects through the creation of eddy currents in the given object. Eddy currents that interact with a magnetic field depend upon the material being examined. A system was assembled, in order to investigate this interaction, that consisted of an excitation source and a magnetic field sensor. The expected fields and underlying theory are found in Section 2 of this paper. Multiple methods for creating oscillating magnetic fields at a desired frequency were considered. The excitation source chosen as well as other system components can be found in Section 3. Once constructed, testing was done in a sandbox with various targets. The testing methods and results can be found in Sections 4 and 5, respectively.

#### 2. ACTIVE MAGNETIC SENSING

The concept being proposed is that by applying low-frequency magnetic fields to different targets, of both ferromagnetic and non-ferromagnetic composition, the targets will exhibit different magnetic signatures. The oscillating magnetic field will interact with the subject material in different ways depending upon the materials properties, which in turn produces a detectable external magnetic field disturbance.

Further author information:

D.H.: E-mail: Dryver.Huston@uvm.edu, Telephone:1-802-656-1922

# 2.1 Eddy Currents

A non-ferromagnetic electrically conductive material placed in the presence of an alternating electromagnetic field will experience some degree of penetration from the applied electromagnetic field. With this penetration, eddy currents are generated in the material. When present, these continuous eddy currents provide a magnetic field that generally opposes the applied field, resulting in a decrease in the amplitude of the electromagnetic field near the target. The greater the intensity of the eddy current, the greater the opposition to the applied electromagnetic field.<sup>3</sup> In order for the presence of the eddy currents to be detected, the strength of the magnetic field created by the eddy current should be maximized.

The application of an alternating electromagnetic field to ferromagnetic materials results in a concentration of the initially applied field, likely mitigating any observable impacts on the magnetic field from the creation of eddy currents. Two material properties that have a significant impact on the strength of the eddy current are electrical conductivity and magnetic permeability. A material with a high electrical conductivity results in more intense eddy current formulation than that of a material with a low electrical conductivity. With regards to magnetic permeability, metals can be broken into three main groups, paramagnetic, diamagnetic and ferromagnetic. Paramagnetic materials have a relative magnetic permeability of just greater than 1, diamagnetic materials exhibit relative magnetic permeability values of less than 1, while ferromagnetic materials generally have a relative magnetic permeability of much greater than 1. If a material has a relative magnetic permeability of less than 1, it exhibits slight opposition to applied magnetic fields. High magnetic permeability results in a general decrease in the penetration depth.<sup>4</sup>

Penetration depth in itself is another critical parameter to the formulation of eddy currents in a conductor. The penetration depth is defined as

$$\delta = \sqrt{\frac{2}{\mu\omega\sigma}},\tag{1}$$

where  $\mu$ ,  $\omega$  and  $\sigma$  are the magnetic permeability, electromagnetic field oscillation frequency and the electrical conductivity of the material, respectively.<sup>5</sup> Values of estimated penetration depth for general aluminum and copper were calculated using their material properties and a magnetic field frequency of 210 Hz<sup>6,7</sup>. The penetration depth for aluminum and copper were found to be 14.2 mm and 10.4 mm, respectively. It is apparent that lower frequency applied electromagnetic fields yield a greater penetration depth into the material of interest. However, when attempting to tune the applied frequency, the skin effect can alter the distribution of the reactionary fields within the solid. In general, eddy currents may appear on the opposite side of the test piece if the material thickness is not at least three times that of the standard penetration depth.<sup>4</sup> This is important to consider with regard to the material thickness of the target under examination. For this proposed sensing technique, applied magnetic field oscillation frequencies in the range of 200 Hz are examined. A standard range for testing that involves the examination of induced eddy currents is 100 Hz to 10 MHz.<sup>8</sup>

# 2.2 Magnetic Field Definition

The static vector field of a magnetic point dipole can be defined as

$$\mathbf{B} = -\frac{\mathbf{M}}{R^3} + (3\mathbf{M} \cdot \mathbf{R}) \, \frac{\mathbf{R}}{R^5},\tag{2}$$

where  $\mathbf{R}$  is the radius vector from the point dipole to some point, R is the magnitude of  $\mathbf{R}$ ,  $\mathbf{M}$  is the magnetic moment vector and  $\mathbf{B}$  is the magnetic induction vector. This equation can be reduced to the commonly used simple scalar representation

$$B \approx \frac{M}{R^3},$$
 (3)

where it can be seen that the magnetic field strength attenuates proportional to the inverse of distance cubed. This is an important relation to consider in the orientation of any magnetic sensing system. The proximity of both the excitation source and the sensor to the target needs to be intentional with regards to the field strength in order for changes in the field to be measurable. A static representation of this field for two in phase cylindrical dipole magnets can be seen in Fig. 1 below.

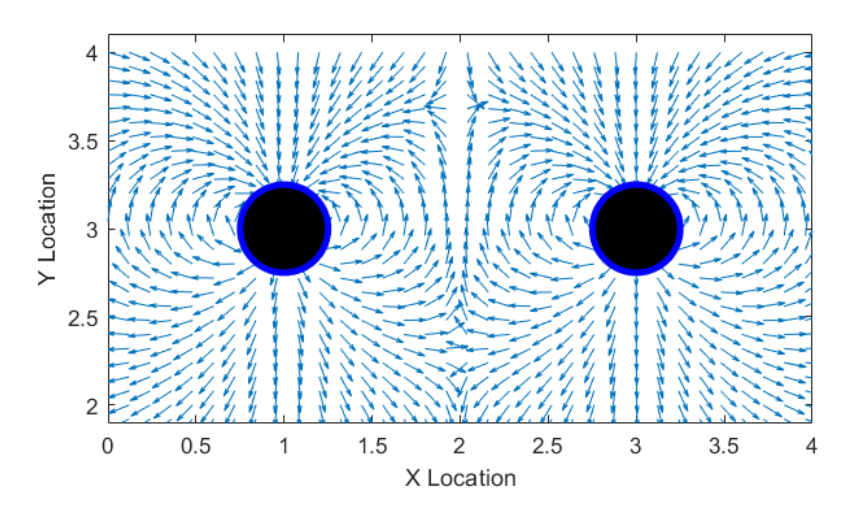


Figure 1: Mathematical model of two in phase cylindrical dipole magnets. The arrows represent local direction vectors of the magnetic field at given points in space.

The concept of dual rotating dipole magnets will be expanded upon later in this paper. Dual rotating magnets, as opposed to a singular rotating magnet, have been proven to be effective in projecting strong magnetic fields. <sup>10</sup> Another concept that will be expanded upon in this paper is the use of multipole magnets rather than dipole magnets.

#### 3. ACTIVE MAGNETIC SENSING SYSTEM DESIGN

## 3.1 Oscillating Magnetic Field Generation

In order to detect the presence of a non-ferromagnetic object, there must be a magnetic excitation source that is capable of inducing eddy currents and sensors that can detect the resulting field disturbance. There are two main methods for creating an alternating magnetic field, the most common being an alternating current through a coil. This projects a magnetic field, however the coils can be very large and power intensive. <sup>11</sup> An alternate method is to rotate a magnet that has alternating radial poles. With advancements in compact neodymium magnets, this method can provide strong alternating magnetic fields with low power consumption. The potential downside to this method is frequency limitations due to mechanical considerations. That being said, there are approaches in which magnetic field oscillation frequencies can reach up to 210 Hz without the need for high speed motors. With a traditional dipole magnet, this would require a motor to spin up to 210 Hz, which can become costly and power intensive. The solution to this problem that is used in this paper is a multipole magnet with radially alternating poles. A 12 pole magnet has 6 north and 6 south poles facing outward around its circumference and could be modelled as 6 dipole magnets in a convenient arrangement. This means that magnetic field oscillation frequencies of 6 times the frequency ability of the motor being used can be achieved. Fig. 2 shows the 12 pole magnet used, its pole identification and a magnetic characterization using indicator paper. The magnet is composed of 12 Neodymium 50H wedge magnets and housed within a brass cylinder. The outer diameter of the magnet is 25.4 mm and the depth is 12.7 mm. The indicator paper displays the magnitude of the magnetic field and has no indication of north versus south poles. Rotating this multipole magnet will ideally result in a projecting alternating magnetic field, meaning that if the magnetic field is sensed at a tangential orientation to the rotating magnet, a sine wave could be observed.

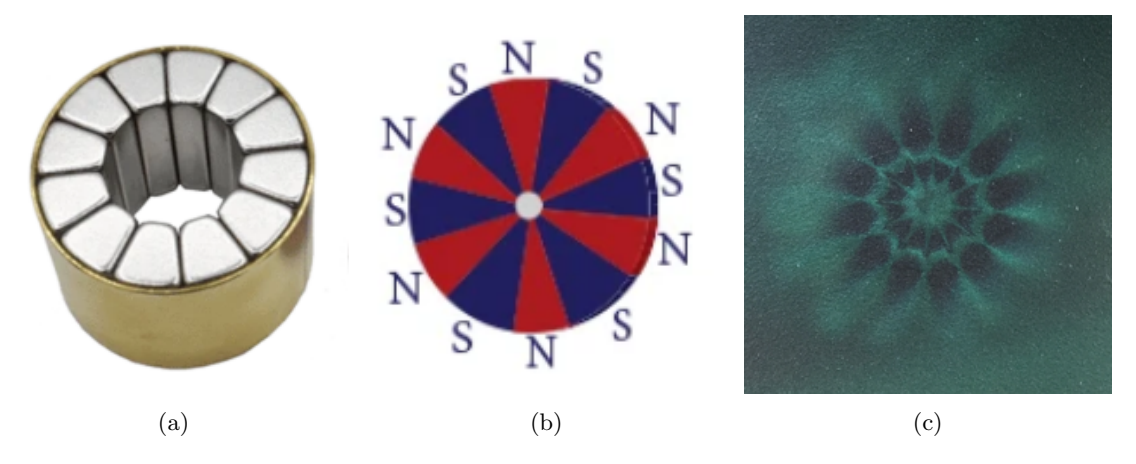


Figure 2: Multipole magnet with radially alternating poles (a), pole identification for this particular magnet (b), and the magnetic field characterization using magnetic indicator paper (c).

The following system components enable the precise motion control as required for the implementation of these multipole magnets. A dual rotating magnet concept provided the most effective magnetic field propagation. Two Galil servo motors were used for the rotation of the two magnets. In order to maintain precise phase control, electronic gearing methods were implemented through use of a 2-axis Galil DMC4123 motion controller. In Fig. 3 below, both the motion controller and the motor used can be seen.



Figure 3: Galil 2-axis motion controller (a) and Galil servo motor used to spin the magnets (b).

## 3.2 Magnetic Field Sensing

The magnetometer used for sensing magnetic field values in this paper is the PNI RM3100. This magnetometer senses the magnetic field present in 3 axes at up to 533 samples per second in each axis. All data collected for this paper was done so with the magnetometer sampling at 480 Hz in each of the 3 axes. At this sample frequency, the magnetometer maintains a sensitivity of 50 nanoteslas. Three axes are sampled through the incorporation of three sensing coils oriented orthogonal to each other. The layout of these sensing coils can be visualized in Fig. 4 below. Pairing the magnetometer with an STM32 Nucleo-F411RE development board establishes USB data transmission from the magnetometer.

#### 3.3 Component Configuration

In Fig. 5 below, the assembled system with a clear housing can be seen. The magnetometer placement is directly between the two motors and on the underside of the housing. This location enables the magnetometer to pick

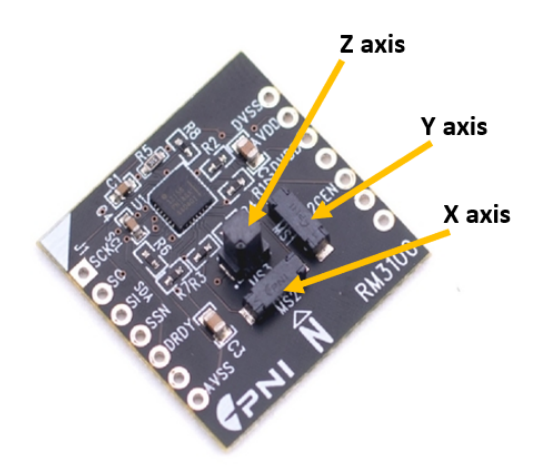


Figure 4: PNI RM3100 magnetometer with the three orthogonal sensing coils identified.

up on changes in the magnetic field caused by an object that passes below the system. With this configuration, the system can be translated over a surface, while recording data, and the data can be analyzed to determine the presence of an object capable of interacting with magnetic fields at a given frequency.

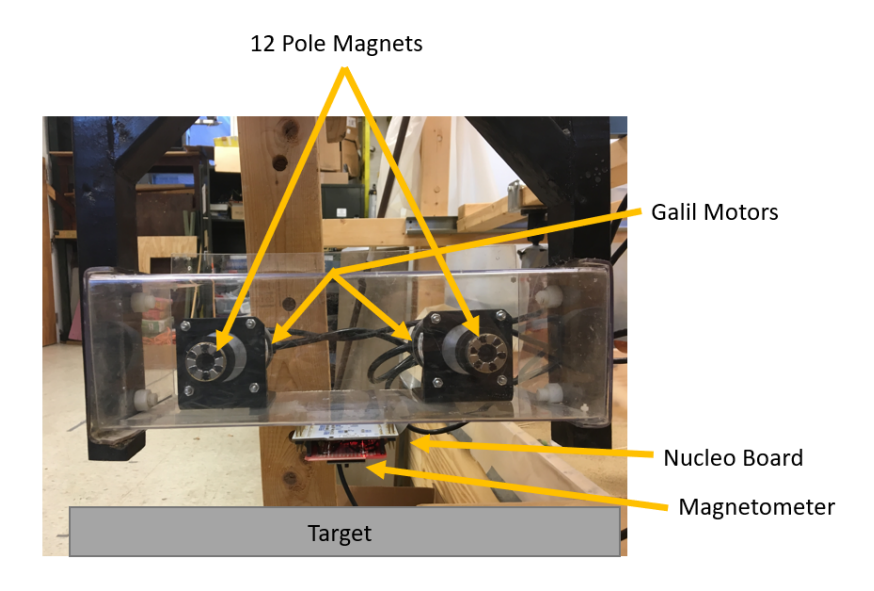


Figure 5: The two Galil motors with two 12 pole magnets mounted to the shafts. The magnetometer interfaces with the STM32 Nucleo-F411RE development board with a placement directly between the two motors on the underside of the housing.

#### 4. DATA COLLECTION

## 4.1 Methods

All testing was completed in a 3 meter by 3 meter sandbox that contains 190 mm of sand. The active magnetic sensing system was suspended so that the magnetometer was 50 mm above the surface of the sand. The system was then translated 1.17 m across the sandbox at a speed of 36 mm/s. The sandbox with the active magnetic sensing system can be visualized in Fig. 6 below. Targets of various materials and dimensions were placed on the surface of the sand perpendicular to, but in the path of, the scan direction that is represented by the red arrow.

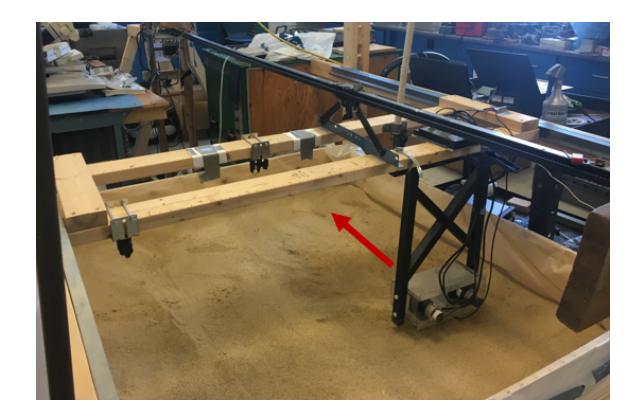


Figure 6: The active magnetic sensing system is translated along the axis of the red arrow at a constant speed.

# 4.2 Targets

A number of targets were examined in scans across the sandbox at a variety of magnetic field oscillation frequencies. These targets vary in geometry and composition. The primary materials under examination are aluminum, steel and copper. Three key targets can be seen in Fig. 7 below. The ends are covered on each of these pipes in order to prevent them from filling up with sand during testing. The wall thickness of each of these pipes varies. While this thickness has an impact on the interaction of eddy currents, it is not common to have a steel pipe of the same wall thickness as a copper pipe. Copper is likely to have thin walls while steel and aluminum are likely to have a larger wall thickness, which is exhibited in these pipe samples. Three additional targets of interest are an inert anti-personnel landmine, rock of similar size to the landmine and an aluminum disc, of which can be seen in Fig. 8 below.

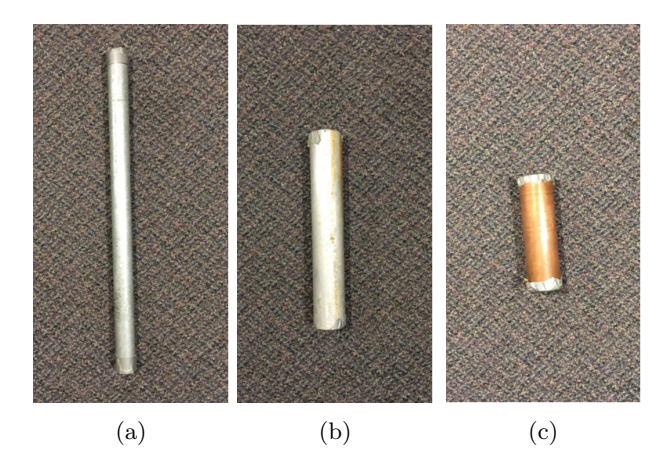


Figure 7: Pictured is a 32 mm OD steel pipe that is 530 mm long (a), a 50 mm OD aluminum pipe that is 305 mm long (b) and a 50 mm OD copper pipe that is 178 mm long (c).

# 5. RESULTS

#### 5.1 Magnetic Field Oscillation Frequency

The most successful configuration for the scans across the sandbox was found to be with the motors spinning in opposite directions with the magnets in phase with each other. The frequency used for inducing eddy currents in non-ferromagnetic materials was a 35 Hz motor frequency, theoretically resulting in a magnetic field oscillation frequency of 210 Hz. This is approaching the maximum acceptable field frequency when sampling at 480 Hz. In order to verify that this model holds true for two counter-rotating multipole magnets, a frequency analysis

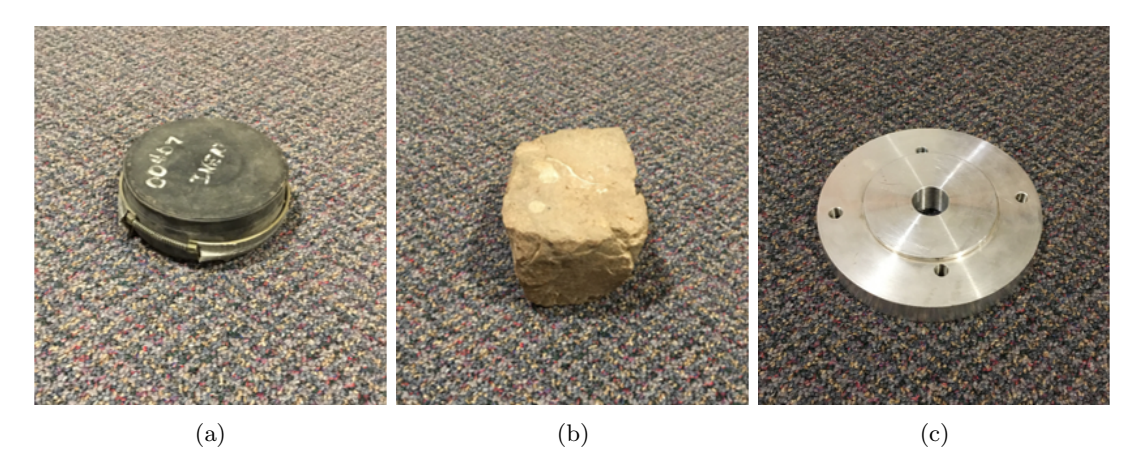


Figure 8: Pictured is a 101 mm OD inert anti-personnel landmine (a), rock of undetermined make up and approximate size to the landmine (b) and a 152 mm OD aluminum disc with a 20 mm thickness(c).

was conducted on a large sample of magnetic data while the magnets were in motion. Because the magnets have 12 poles, it is expected that the magnetic fields oscillation frequency is six times that of the motor rotation frequency. This examination can be seen in Fig. 9 below. The plots were created utilizing the fast Fourier transform function in MATLAB. The signal was smoothed using Welch's power spectral density estimate, which was calculated utilizing a Nuttall-defined Blackman-Harris window. The peak at the desired frequency is called out using an arrow. However, a number of lower frequency peaks can also be visualized at multiples of the motor speed, likely due to slight imbalances in the wedge magnets that the multipole magnet is composed of. The peaks appear to be following a non-linear system sub-harmonics trend from the motor frequency until the larger 210 Hz peak.<sup>12</sup>

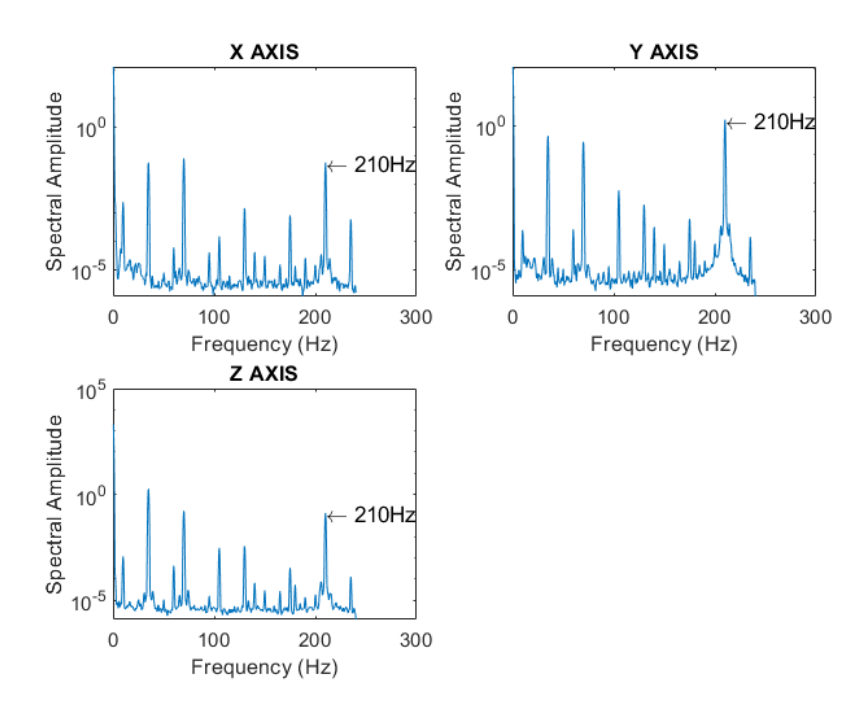


Figure 9: Fast Fourier transform of data where both motors are spinning the multipole magnets at 35 Hz in opposite directions. Plots for all three of the magnetometer axes have a logarithmic y axis.

#### 5.2 Sandbox Scans

Each of the targets were placed around 0.75-0.85 m from the beginning of the scan and the system was translated over the top of each target with each target placed on the surface of the sand. The red lines on each of the plots below in Figs. 10, 11 and 12 represent the location of the center of the pipe along the scan. A background subtraction from the raw data was completed. These plots show the results from the sampling in the Z axis coil. This is the direction in which the greatest impact from all of the scan targets can be visualized. It can be seen that the oscillating magnetic field signal experiences a decrease in amplitude as it passes over the aluminum pipe in Fig. 10(a). In order to examine the magnetic signal being recorded, Fig. 10(b) shows a zoomed in view of the scan at a trivial location along the scan. It can be observed that the magnetic field is indeed oscillating as predicted. However, additional oscillations can be seen within the sine wave. These additional oscillations represent the 210 Hz frequency detected in previous fast Fourier transform.

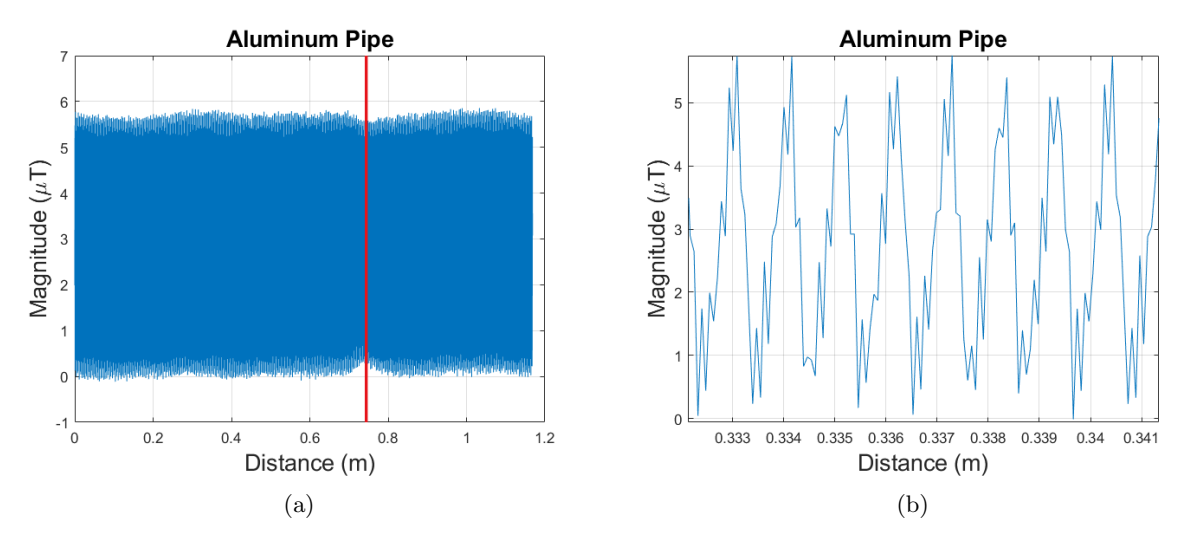


Figure 10: Magnetic signal sensed in the Z axis for a scan over the sand box with the aluminum pipe present (a) and a view of the signal being sensed during the scan (b).

In order to analyze changes in the magnetic field, a peak based envelope averaged over every 630 samples was calculated in MATLAB. This sample averaging value was chosen because it is three times the expected oscillation frequency. The blue lines in Fig 11 below represent this mentioned envelope. It is evident that the presence of steel provides a drastically different interference with the applied magnetic field than that of the aluminum and copper. The presence of steel results in a change in the average value for which the magnetic field is oscillating about. The aluminum and copper create a slight decrease in the amplitude of the magnetic field, indicating that these materials create a magnetic field of their own that opposes the applied magnetic field.

The same procedure was followed for comparing the landmine, rock and aluminum disc. The red line indicates the location of the center of the target. These results can be seen in Fig. 12 below. The plots indicate that the larger thickness of this aluminum disc may contribute to a stronger opposing magnetic field present in the aluminum disc than that of the aluminum pipe previously examined. It can also be observed that the landmine has a similar influence as that of the steel pipe, where the upper and lower envelopes are identical, rather than mirrors of each other as seen in the aluminum plot. This is likely due to a small steel spring that is located on the exterior of the landmine. The rock exhibits no detectable influence on the detected magnetic field.

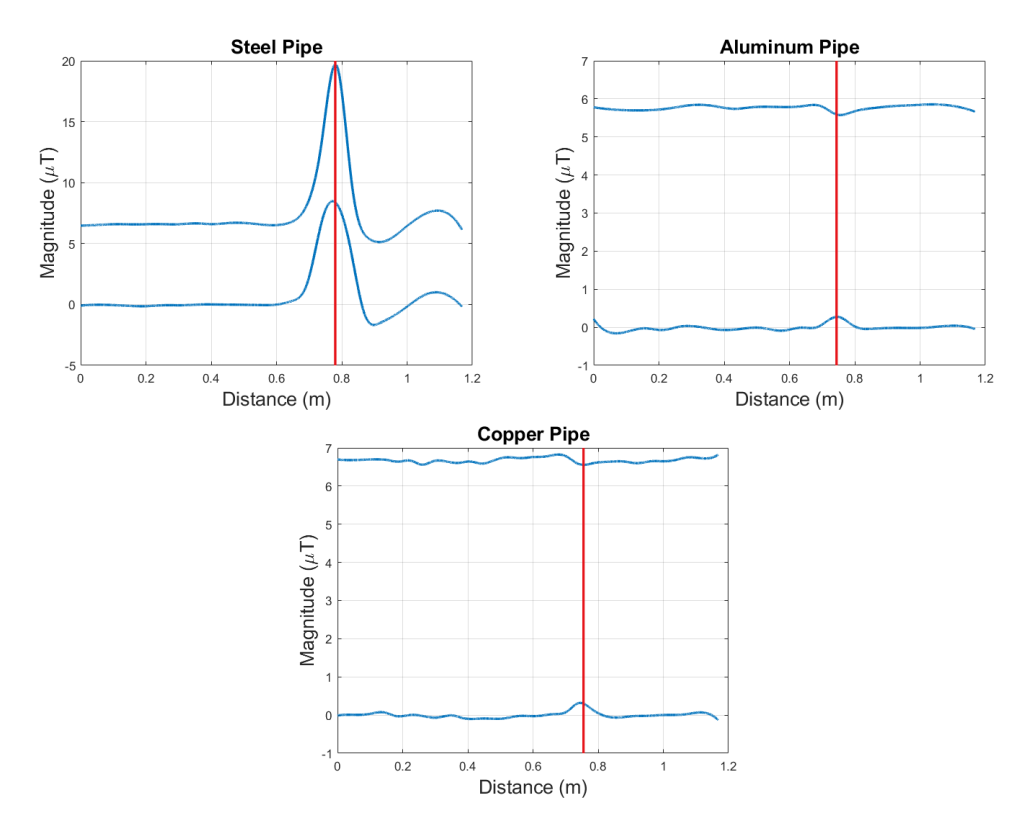


Figure 11: Scans over the sand box with the respective pipe present as labelled on each plot.

# 6. CONCLUSION

The results indicate that eddy currents can be induced in a conductive metal through the use of rotating permanent multipole magnets. Non-ferromagnetic metals have been successfully detected using a magnetic sensing device due to the opposing magnetic field generated by these eddy currents. A compact geomagnetic magnetometer was successfully used for the detection of eddy currents in conductive materials. Multipole permanent magnets were also a successful method for increasing the frequency of oscillating magnetic fields without introducing high speed motors or large power intensive coils. However, the frequency of the motor and sub-multiples of this frequency were also detected during testing. This is likely a result of slight imbalances of each individual wedge magnet. The interaction of ferromagnetic materials and the oscillating magnetic field produced a distinct feature in which the average value of the magnetic field present is changed, whereas the non-ferromagnetic materials exhibited an amplitude change about the same axis of oscillation. The inert landmine could also clearly be differentiated from a rock, as the rock has no magnetic influence. While underground investigation was not completed in this study, larger magnets with a larger pull force may be desirable for sensing of greater depths. Further target examination may also be of interest such as lead pipes or rocks of different composition for comparison to the landmine.

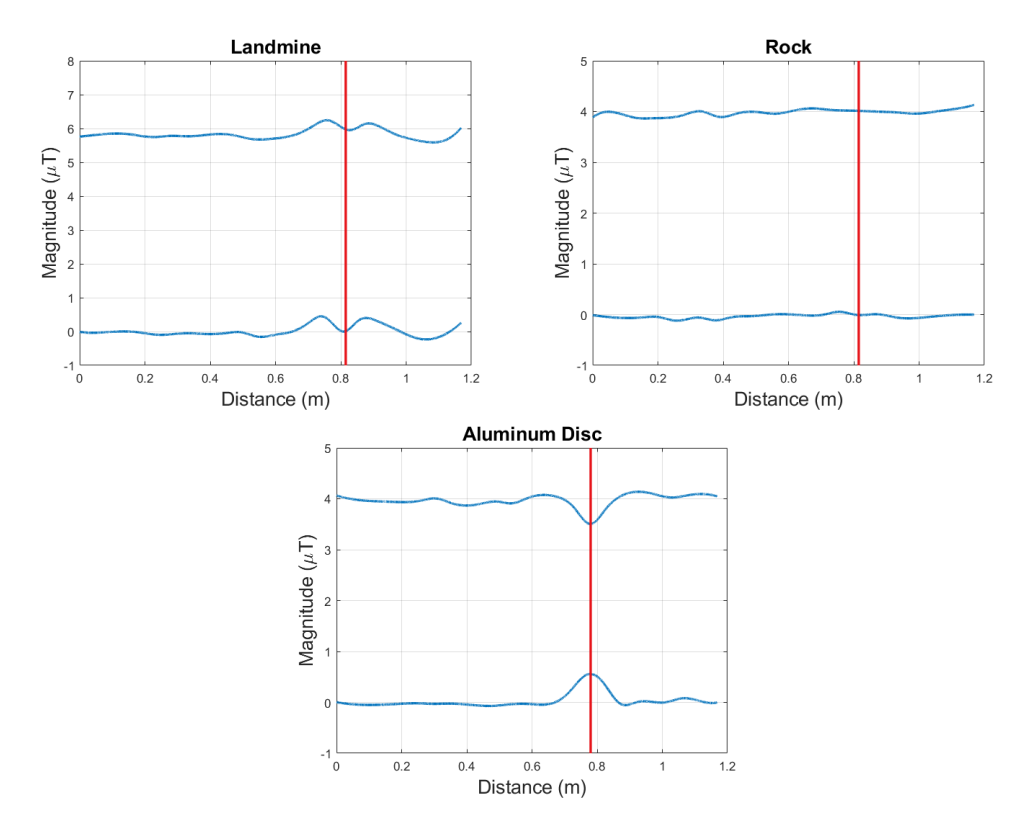


Figure 12: Scans over the sand box with the respective targets present as labelled on each plot.

## ACKNOWLEDGMENTS

This work has been supported by the U.S. Army W911NF-17-C-0082 with White River Technologies, the National Science Foundation in grants 1647096 and 1640687, and the University of Vermont SPARK Fund.

## REFERENCES

- [1] Huuskonen-Snicker, E., Mikhnev, V. A., and Olkkonen, M., "Discrimination of buried objects in impulse gpr using phase retrieval technique," *IEEE Transactions on Geoscience and Remote Sensing* **53**(2), 1001–1007 (2015).
- [2] Savelyev, T. G., van Kempen, L., Sahli, H., Sachs, J., and Sato, M., "Investigation of time-frequency features for gpr landmine discrimination," *IEEE Transactions on Geoscience and Remote Sensing* **45**(1), 118–129 (2007).
- [3] Placko, D. and Dufour, I., "Eddy current sensors for nondestructive inspection of graphite composite materials," in [Conference Record of the 1992 IEEE Industry Applications Society Annual Meeting], 1676–1682 vol.2 (1992).
- [4] García-Martín, J., Gómez-Gil, J., and Vásquez-Sánchez, E., "Non-destructive techniques based on eddy current testing," Sensors 11, 2525–2565 (2011).
- [5] Ramos, H. M. G., Postolache, O., Alegria, F. C., and Lopes Ribeiro, A., "Using the skin effect to estimate cracks depths in mettalic structures," in [2009 IEEE Instrumentation and Measurement Technology Conference], 1361–1366 (2009).
- [6] "Electrical Conductivity of Elements and other Materials." Engineering Toolbox, 2008 https://www.engineeringtoolbox.com/conductors-d\_1381.html. (Accessed: 30 March 2020).
- [7] "Permeability." Engineering Toolbox, 2016 https://www.engineeringtoolbox.com/permeability-d\_1923.html. (Accessed: 30 March 2020).

- [8] Ditchburn, R., Burke, S., and Posada, M., "Eddy-current nondestructive inspection with thin spiral coils: Long cracks in steel," *Journal of Nondestructive Evaluation* **22**, 63–77 (2003).
- [9] Moser, P., "Magnetic signatures of submarines I," tech. rep., Pacific-Sierra Research Group (1994).
- [10] Farrell, R., Rotating magnetometry for terrestrial and extraterrestrial subsurface explorations, Master's thesis, University of Vermont (2018).
- [11] Norton, S. J. and Won, I. J., "Identification of buried unexploded ordnance from broadband electromagnetic induction data," *IEEE Trans. Geoscience and Remote Sensing* **39**, 2253–2261 (2001).
- [12] Peng, Z., Lang, Z., Billings, S., and Tomlinson, G., "Comparisons between harmonic balance and nonlinear outputfrequency response function in nonlinear system analysis," *Elsevier Journal of Sound and Vibration* **311**, 56–73 (2008).